

## Comparison of brain functions between healthy participants and methamphetamine users with various addiction histories: Data analysis based on EEG and fNIRS

Xuelin Gu , Xiaou Li \*,<sup>†</sup> and Banghua Yang †,§

\*College of Medical Instruments, Shanghai University of Medicine & Health Sciences, Shanghai 201318, P. R. China

†School of Mechanical and Electrical Engineering and Automation, Shanghai University, Shanghai 200444, P. R. China

<sup>\*</sup>[lixo@sumhs.edu.cn](mailto:lixo@sumhs.edu.cn)

<sup>§</sup>[yangbanghua@shu.edu.cn](mailto:yangbanghua@shu.edu.cn)

Received 15 July 2023

Accepted 22 October 2023

Published 20 January 2024

The electroencephalogram (EEG) rhythm and functional near-infrared spectroscopy (fNIRS) activation levels have not been compared between a healthy control group (HCG) and methamphetamine user group (MUG) with different addiction histories. This study used 64-electrode EEG and fNIRS to conduct an experiment that analyzed the resting and craving states. The EEG and fNIRS data of 56 participants were collected, including 14 healthy participants, 14 methamphetamine users with an addiction history of 0.5–5 years, 14 users with an addiction history of 5–10 years, and 14 users with an addiction history of 10–15 years. Isolated effective coherence (iCoh) within the brain network was used to process the EEG data. Statistical analysis was performed to compare differences in iCoh among the delta, theta, alpha, beta, and gamma bands and explore oxyhemoglobin activation levels in the ventrolateral prefrontal cortex, dorsolateral prefrontal cortex, orbitofrontal cortex, and frontopolar prefrontal cortex (FPC) of the control group. Finally, the Kmeans, Gaussian mixed model (GMM), linear discriminant analysis (LDA), support vector machine (SVM), Bayes, and convolutional neural networks (CNN) algorithms were used to classify methamphetamine users based on drug and neutral images. A 3-class accuracy was achieved. Changes in EEG and fNIRS activation levels of HCG and MUG with varied addiction histories were demonstrated.

**Keywords:** Drug addiction history; electroencephalogram; functional near-infrared spectroscopy; isolated effective coherence; addiction history classification.

\*§Corresponding authors.

## 1. Introduction

Differences in the electroencephalogram (EEG) rhythm and brain activation levels between healthy participants and methamphetamine users reveal the physiological evolution of the brain after addiction. This research had six objectives: (1) Obtaining the EEG and fNIRS data of 56 healthy participants and methamphetamine users; (2) classifying Kmeans, Gaussian mixed model (GMM), linear discriminant analysis (LDA), support vector machine (SVM), Bayes, and the convolutional neural networks (CNN) algorithms based on the drug and neutral image data; (3) developing the isolated effective coherence (iCoh) brain network to analyze the differences between the healthy and addiction groups; (4) reviewing energy changes in the brain electrical activity map of the control group in the resting state when participants opened and closed their eyes; (5) analyzing the brain activation level in the frontopolar prefrontal cortex (FPC) of the healthy participants and methamphetamine users; and (6) generating a three-dimensional activation map of the healthy and addiction groups.

EEG refers to the autonomous bioelectric signals of neurons collected from the scalp. EEG has a time resolution of milliseconds and measures changes in brain neurophysiology.<sup>1,2</sup> Functional near-infrared spectroscopy (fNIRS) is a spectral measurement tool based on detection at the scalp. fNIRS measures blood dynamics at optical injection and detection points and records blood oxygen levels.<sup>3,4</sup>

The human brain comprises an interactive network with complex structures and functions that facilitate information isolation and integrate various cognitive functions.<sup>5,6</sup> Most studies that analyze electrophysiological signals are based on sensing or source layer analyses and combine EEG with advanced coupling approaches, thereby yielding valuable functional information.<sup>7,8</sup> The imaginary part of coherence (iCoh) is not sensitive to the brain volume effect and removes all indirect causality, thereby accurately assessing the direct causality among the nodes in the brain network. Most studies have used iCoh to investigate psychological diseases, such as Alzheimer's disease and autism.<sup>9-11</sup>

A literature review conducted by Ehlis *et al.* on fNIRS in different neuropsychiatric disorders demonstrated the potential of fNIRS in future research.<sup>12</sup> Huhn *et al.* used fNIRS to objectively evaluate methadone clinics and reported that

opioids affect depressive symptoms and drug cravings.<sup>13</sup> Stewart *et al.* showed that there are no effective interventions for opioid use disorder, which imposes a heavy burden on public health. These studies proposed various physiological and neural mechanisms instantiating this cycle of negative reinforcement in drug users. Hada *et al.* used fNIRS to study the brain network and discovered problems with the functions of the orbitofrontal cortex (OFC) in heroin addicts.<sup>14</sup> Lena *et al.* used fNIRS to design the Approach Avoidance Task and determined the role of alcohol dependence in emotion regulation.<sup>15</sup> Okada *et al.* used an fNIRS device to study methamphetamine abuse and arrived at the common underwater pathophysiology of methamphetamine-associated psychosis and schizophrenia.<sup>16</sup>

Methamphetamine has the largest use and addiction populations worldwide. Changes in the brain caused by methamphetamine addiction can be explored by studying healthy participants and methamphetamine users with various addiction histories. The EEG and fNIRS data of 56 participants were collected. The addiction histories induced by the drug and neutral images were classified with the Kmeans, GMM, LDA, SVM, Bayes, and CNN algorithms. The healthy participants and methamphetamine users were assessed using the iCoh<sup>17</sup> brain network. Brain activation level in the FPC of the healthy participants and methamphetamine users was analyzed. This research is valuable as it reveals the physiological changes in the brain after addiction, and it can be used to design rehabilitation therapies for methamphetamine users.

## 2. Materials and Methods

We used the Kmeans,<sup>18,19</sup> GMM,<sup>20,21</sup> LDA,<sup>22-25</sup> and the generalized naïve Bayes classifier (GNBC) traditional algorithms to classify the different addiction histories.<sup>26-28</sup> We built the CNN classification model used in the classification algorithm. The EEG and fNIRS data were induced by drug maps and neutral maps, respectively. The channels of methamphetamine users in the functional areas of the ventrolateral prefrontal cortex (VLPFC), the dorsolateral prefrontal cortex (DLPFC), the OFC, and the FPC were selected. We verified the difference in the classification accuracy of the four functional areas of the brain to explain this result.

First, the fNIRS data induced by the drug maps and neutral maps were obtained. Second, four brain regions and their corresponding channels were selected and processed using the Kmeans, GMM, LDA, SVM, GNBC, and CNN algorithms. Finally, the difference in the three-class accuracy in the four brain regions induced by the different maps was determined. The processing flow of drug abuse data is shown in Fig. 1.

## 2.1. Traditional algorithm data processing

Kmeans, GMM, LDA, SVM, GMM, and GNBC used the fNIRS data of the VLPFC, DLPFC, OFC, and FPC to classify methamphetamine users. Channels in the four brain regions were selected. Kmeans, GMM, LDA, SVM, and GNBC used the original data as training and test sets. The classification model selected 30 and 12 data points as the training and test sets, respectively, cross-validated the model and performed two classes twice. Finally, we obtain the three-class accuracy.

## 2.2. Machine-learning data processing

(1) Near infrared data are very easy to receive the interference of heartbeat and respiration. In order to retain the characteristics of the original signal to the greatest extent, we use Butterworth filter for filtering. The expression of  $n$ th order Butterworth

filter is as follows:

$$|\mathbf{H}(\mathbf{f})|^2 = \frac{1}{1 + \left(\frac{\mathbf{f}}{\mathbf{f}_c}\right)^{2n}} = \frac{1}{1 + \epsilon^2 \left(\frac{\mathbf{f}}{\mathbf{f}_p}\right)^{2n}}, \quad (1)$$

where  $n$  is the order,  $\mathbf{f}_c$  is the cutoff frequency, and  $\mathbf{f}_p$  is the passband edge frequency.

In this experiment,  $n$  is 6 and the data are band-pass-filtered. The selected frequency band ranges from 0.01 Hz to 3 Hz. This frequency range can remove the interference of heartbeat breathing and slow drift on the original data, and can also retain the characteristics related to the drug addiction.

CNN was only used in the field of image recognition in the early days, and obtained very good classification results. In the subsequent development, it was gradually applied to signal processing, and it has a good classification effect in the field of biological signal analysis. The focus of this paper is to design a reasonable and effective DS-CNN\_SE structure to better extract features from forehead near infrared data.

Convolutional layers are the core of CNN. Its main role is to extract features from the input data. The calculation form is as follows:

$$x_j^l = f \left( \sum_{i \in M_j} x_i^{l-1} \cdot k_{ij}^l + b_j^l \right). \quad (2)$$

$b_j^l$  is the bias parameter,  $\text{down}()$  is a sub-sampling function,  $f()$  is the activation function; In this paper, the sub-sampling function uses the average

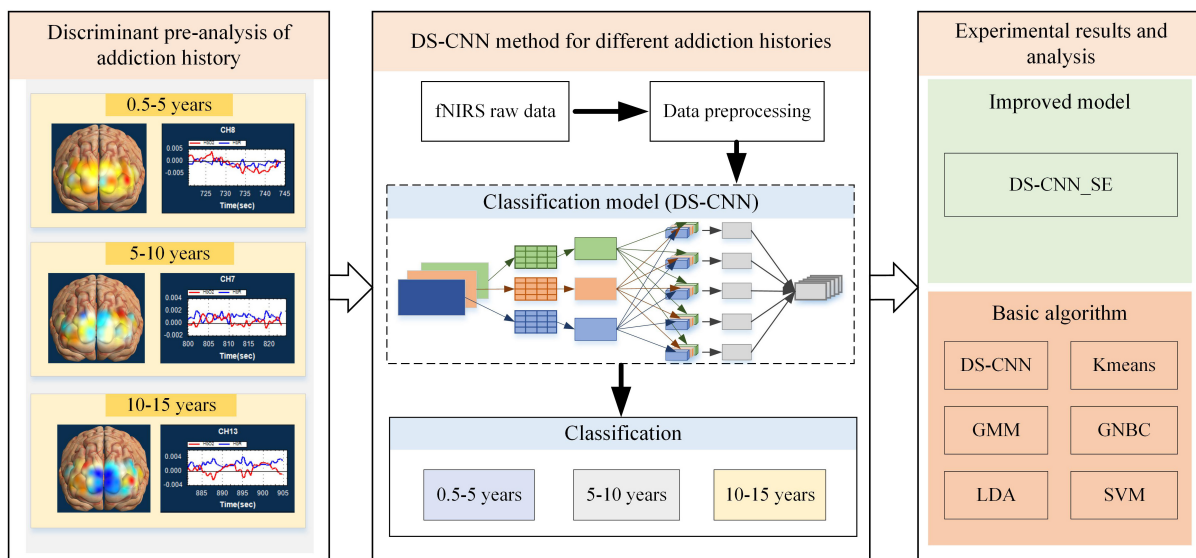


Fig. 1. Data processing flow of traditional algorithm and CNN.

pooling function, so that the hidden information in the data is retained to the maximum extent and the redundant information is reduced. The activation function is an identity function.

(2) Depth wise Separable Convolution: The core idea of Depth wise Separable Convolution is to decompose the standard convolution process into two steps, namely, Depth wise Convolution and Pointwise Convolution.

$$\text{Conv}(W, y)_{(i,j)} = \sum_{k,l,c}^{K,L,C} W_{(k,l,c)} \cdot y_{(i+k,j+l,c)}, \quad (3)$$

$$\text{pconv}(W, y)_{(i,j)} = \sum_c^C W_c \cdot y_{(i,j,c)}, \quad (4)$$

$$\text{dconv}(W, y)_{(i,j)} = \sum_{k,l}^{K,L} W_{(k,l)} \cdot y_{(i+k,j+l)}, \quad (5)$$

$$\begin{aligned} \text{sconv}(W_p, W_d, y)_{(i,j)} \\ = \text{pconv}_{(i,j)}(W_p, \text{dconv}(W_d, y)). \end{aligned} \quad (6)$$

(3) Channel Shuffle Attention Module: This paper proposes a Channel Shuffle Attention Module. Using the Channel Shuffle operation can effectively promote the flow of information between channels, enhance the network's ability to select features, and thereby improve the network's representation ability. As shown in Fig. 2, Channel Shuffle Attention Module mainly consists of three parts: Two  $1 \times 1$

bottleneck blocks, global average pooling, and softmax function.

First,  $H_{lfu}$  passes through the first  $1 \times 1$  The convolutional layer compression channel reduces the amounts of parameters. Then, channels are grouped through a group convolution, and the grouped feature channels undergo channel scrambling operations to achieve the flow of information between channels. Finally, it passes through the second  $1 \times 1$  The convolution layer restores the number of output channels to the number of input channels. The process is as follows:

$$X = F_{r2c}(F_{cf}(F_{gc}(F_{c2r}(H_{lfu}, W_c), W_g)), W_r), \quad (7)$$

where  $F_{cf}(\cdot)$  represents channel scrambling operation.  $F_{r2c}(\cdot)$ ,  $F_{c2r}(\cdot)$ , and  $F_{gc}(\cdot)$  denote  $1 \times 1$  convolution and pointwise convolution group convolution;  $W_r$ ,  $W_c$ , and  $W_g$  are their corresponding weights. Then, assuming  $X = [x_1, x_2, \dots, x_c, \dots, x_C] \in \mathbb{R}^{H \times W \times C}$ , through the global average pooling operation, a channel descriptor with a dimension of  $C$  is obtained, and the  $z$  channel descriptor in  $c$  can be expressed as follows:

$$z_c = G_{\text{gap}}(x_c) = \frac{1}{H \times W} \sum_{i=1}^H \sum_{j=1}^W x_c(i, j), \quad (8)$$

where  $G_{\text{gap}}(\cdot)$  represents global average pooling, and the channel descriptor  $z$  can be seen as a centralized representation of the entire image information, because the averaging operation takes into account

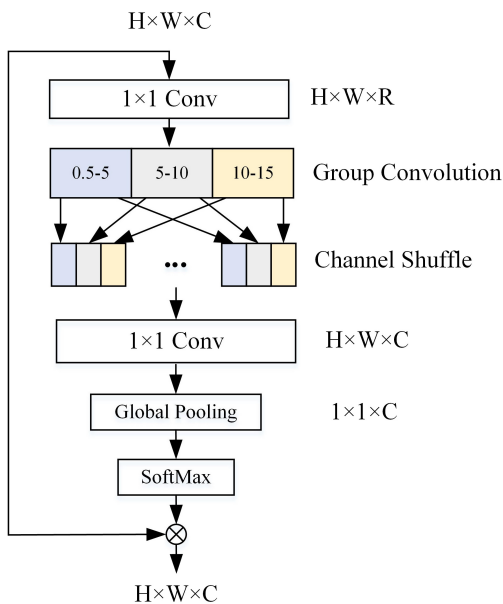


Fig. 2. Channel shuffle attention model.

each pixel in the image. Finally, use the softmax function to calculate the correlation weights between these channel descriptors, namely

$$w = \tau(z) = \frac{e_i^z}{\sum_{i=1}^C e_i^z}, \quad (9)$$

where  $\tau$  represents the softmax function and  $w \in \mathbb{R}^C$  represents the correlation weight with a dimension of  $C$ . Multiplying these correlation weights by the corresponding channels yields the final output of the channel scrambling attention module, which is as follows:

$$\hat{x} = w_c \cdot x_c, \quad (10)$$

where  $w_c$  and  $x_c$  represent the relevant weights and corresponding characteristic channels of the  $c$ th channel.

### 2.3. CNN model decoding and classification

Methamphetamine users in different drug addiction history, 0.5–5 years, 5–10 years, and 10–15 years. Data features: 26 channels, 56 trials for each participant. The data fragment is 6 s after the drug picture appears. CNN model has depth wise convolution and pointwise convolution, and the data input form is time  $\times$  channel. The CNN network including 30 participants training data, 8 validation data, and 4 participants testing data. Since fNIRS equipment uses a frequency of 8.13 Hz, in the 6 second time period, we finally obtain their own 3-class accuracy. We use only depth separable convolutions to mark them as DS-CNN. The channel shuffle attention module added to the

disturbed channel is recorded, marked as DS-CNN\_SE. Figure 3 shows the DS-CNN\_SE classification model.

### 2.4. Experiments

The experimental data originated from healthy and methamphetamine users. The classification accuracy of the methamphetamine users under different addiction histories in the VLPFC, DLPFC, OFC, and FPC functional areas was determined in different brain regions under the induction by different maps. There were differences in the iCoh brain network and EEG topology map between the healthy group and the methamphetamine users. The activation levels in the functional brain regions in the healthy and methamphetamine users' group.

### 2.5. Equipment information

NIRSIT (OBELAB, Seoul, Korea), light source type: Dual wavelength VCSEL laser, technical spectrum: CW: wave 780 nm, 850 nm, spatial resolution  $4 \times 4 \text{ mm}^2$ , sampling rate: 8.13 Hz, light source 24, number of detectors: 32, and detection depth: 1.5 cm. The combination of the distance between different channels and the detection depth of different light sources can form 204 channels. The device wearing method is shown in Fig. 4.

### 2.6. Participant description

Methamphetamine use, type of drug use, drug history, average dose, and frequency of drug use were asked and recorded. The final time of drug use was

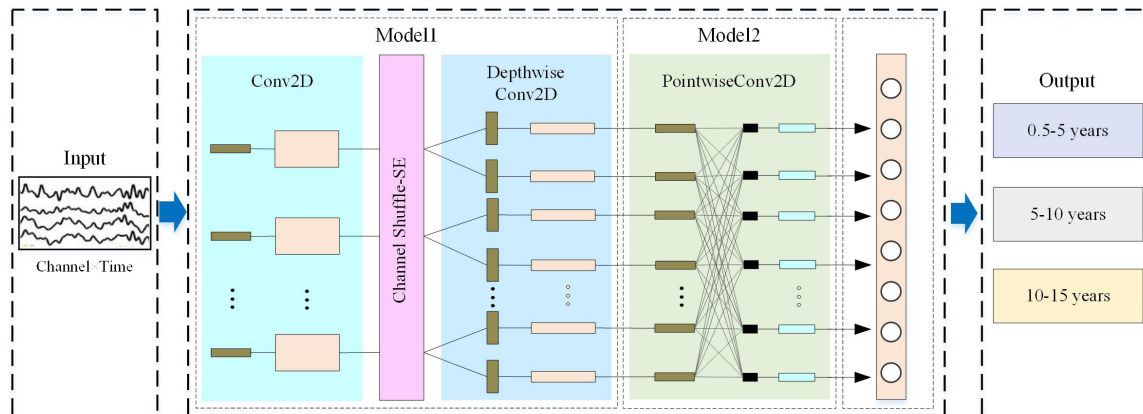


Fig. 3. DS-CNN\_SE classification model.



Fig. 4. Equipment wearing method.

determined with the information data issued by the hospital. The study was conducted in accordance with the declaration of Helsinki and was approved by the Ethics Committee of Shanghai University (Approval No. ECSHU2020-071). The specific information is shown in Table 1.

## 2.7. Dataset

We used E-prime software package (Psychology Software Tools, Pittsburgh, PA) to write the experimental paradigm, with each map numbered. Figure 5 shows the examples of neutral maps and

Fig. 6 shows the examples of drug abuse-related maps used in the experimental paradigm. Figure 7 shows the whole process of experimental paradigm.  $P$  means drug map;  $N$  means neutral map. The first stage of the experimental paradigm lasts 10 min in total, during which the participants need to close their eyes for 5 min and then open their eyes for 5 min.

The second stage lasts 6.28 min and is divided into drug maps and neutral maps. Among them, each block lasts 10 s. There are a total of 16 maps and the display time of each map is 0.6 s. At the beginning, the first four maps are displayed randomly, during which there are two drug maps.

Table 1. Basic information of participants.

Gender	Male
Age range (years)	20–40
Years of education (years)	$10 \pm 1.64$
Weekly usage frequency (times/week)	3–5
Withdrawal time (years)	$1.4 \pm 0.31$
Reasons for drug abuse	sex, decompression, emotion, curiosity



Fig. 5. The example of neutral maps.

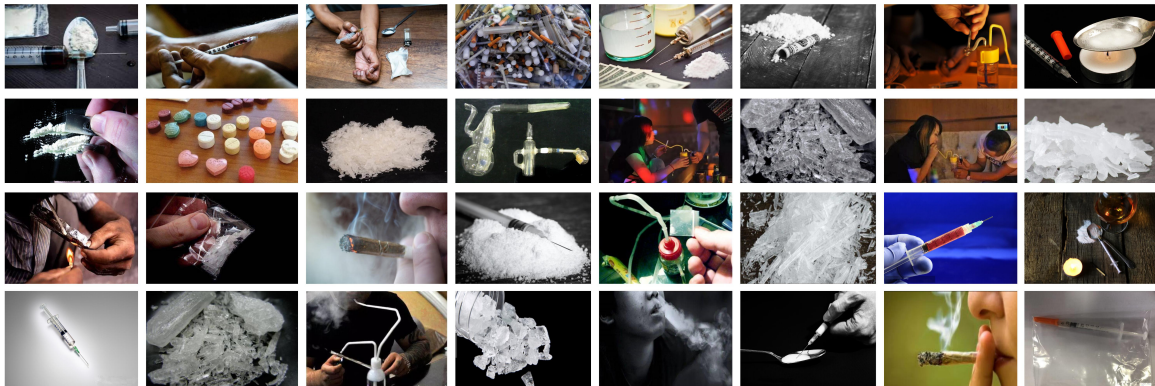


Fig. 6. The example of drug abuse-related maps.

After displaying the first four maps, the remaining 12 neutral maps are displayed randomly. After a block ends, there will be a 4s interval map with a white background and a black cross.

The third stage lasts a total of 4.69 min during which the maps are all neutral with each block lasting 10s. There are 16 maps in total with a display speed of 0.6 s. There will be a 4s interval between each block.

### 3. Results

#### 3.1. The 3-class accuracy of Kmeans, GMM, LDA, SVM, GNBC, and DS-CNN-SE under different addiction history

Kmeans, GMM, LDA, SVM, GNBC, DS-CNN, and DS-CNN\_SE use the fNIRS data of the VLPFC, DLPFC, OFC, FPC for classification.

(1) Under the induction of drug map, the acquired experimental data are processed:

VLPFC: The classification accuracy of Kmeans is stable between 52% and 68%. The classification accuracy of GMM is stable between 51% and 59%. The classification accuracy of GNBC is stable between 43% and 49%. The classification accuracy of SVM is stable between 50% and 60%. The classification accuracy of LDA is stable between 40% and 49%. The classification accuracy of Bayes is stable between 50% and 58%. The classification accuracy of DS-CNN is stable between 68% and 74%. The classification accuracy of DS-CNN\_SE is stable between 71% and 80%.

DLPFC: The classification accuracy of Kmeans is stable between 53% and 60%. The classification accuracy of GMM is stable between 51% and 55%. The classification accuracy of GNBC is stable between 52% and 60%. The classification accuracy of LDA is stable between 40% and 45%. The classification

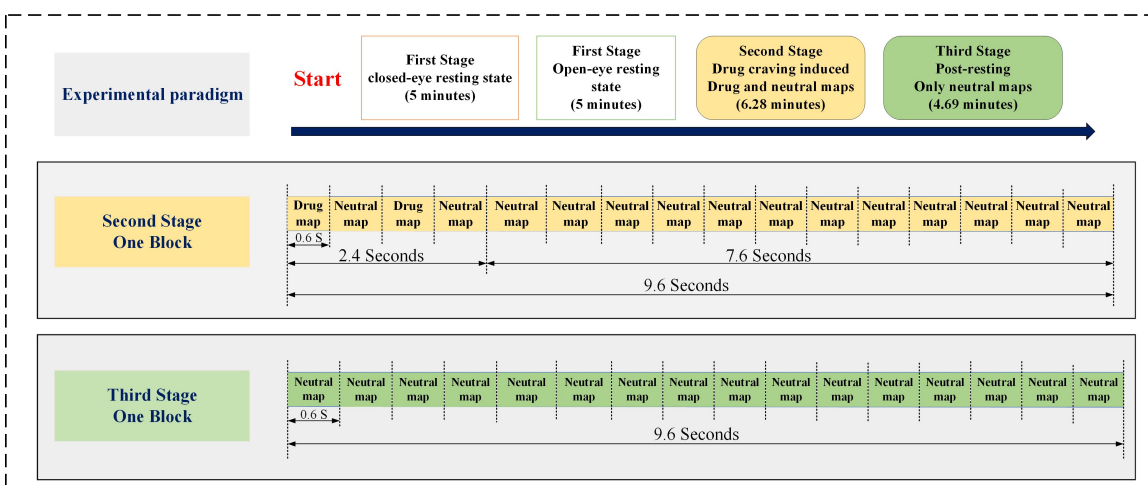


Fig. 7. The whole process of experimental paradigm.

accuracy of SVM is stable between 51% and 60%. The classification accuracy of Bayes is stable between 61% and 66%. The classification accuracy of DS-CNN is stable between 69% and 74%. The classification accuracy of DS-CNN\_SE is stable between 71% and 87%.

OFC: The classification accuracy of Kmeans is stable between 50% and 60%. The classification accuracy of GMM is stable between 50% and 59%. The classification accuracy of GNBC is stable between 51% and 59%. The classification accuracy of LDA is stable between 51% and 58%. The classification accuracy of SVM is stable between 51% and 70%. The classification accuracy of Bayes is stable between 51% and 60%. The classification accuracy of DS-CNN is stable between 73% and 77%.

The classification accuracy of DS-CNN\_SE is stable between 81% and 89%.

FPC: The classification accuracy of Kmeans is stable between 51% and 60%. The classification accuracy of GMM is stable between 56% and 60%. The classification accuracy of GNBC is stable between 51% and 58%. The classification accuracy of LDA is stable between 50% and 56%. The classification accuracy of SVM is stable between 44% and 49%. The classification accuracy of Bayes is stable between 54% and 57%. The classification accuracy of DS-CNN is stable between 74% and 78%. The classification accuracy of DS-CNN\_SE is stable between 84% and 91%. Table 2 shows the 3-class accuracy statistics.

Table 2. 3-class accuracy statistics of drug map introduction.

		1	2	3	4	5	6	7	8	9	10
VLPFC	Kmeans	0.6531	0.5433	0.6620	0.5236	0.6462	0.6872	0.5254	0.6331	0.5643	0.5235
	GMM	0.5826	0.5641	0.5128	0.5646	0.5642	0.5831	0.5728	0.5853	0.5657	0.5426
	GNBC	0.5325	0.5467	0.5326	0.5732	0.5549	0.5643	0.5187	0.5632	0.5341	0.5679
	LDA	0.4885	0.4607	0.4806	0.4806	0.4567	0.4083	0.4567	0.4763	0.4832	0.4349
	SVM	0.4798	0.4865	0.4757	0.4897	0.4983	0.4698	0.4673	0.4797	0.4549	0.4003
	Bayes	0.5373	0.5869	0.5690	0.5690	0.5547	0.5710	0.5016	0.5571	0.5889	0.5750
	DS-CNN	0.7124	0.7361	0.6978	0.7143	0.7283	0.7317	0.6893	0.7194	0.6935	0.6882
	DS-CNN_SE	0.7484	0.7909	0.7234	0.7750	0.7988	0.7651	0.7234	0.7294	0.7155	0.7254
DLPFC	Kmeans	0.5917	0.5733	0.5929	0.5398	0.5869	0.5695	0.5912	0.5653	0.5858	0.5485
	GMM	0.5371	0.5344	0.5436	0.5339	0.5447	0.5328	0.5181	0.5490	0.5338	0.5393
	GNBC	0.5821	0.5456	0.5783	0.5619	0.5294	0.5376	0.5832	0.5618	0.5746	0.5635
	LDA	0.4083	0.4115	0.4480	0.4004	0.4440	0.4984	0.4281	0.4361	0.4183	0.4905
	SVM	0.5917	0.5123	0.5341	0.5115	0.5182	0.5837	0.5043	0.5738	0.5064	0.5638
	Bayes	0.6365	0.6683	0.6325	0.6365	0.6524	0.6206	0.6484	0.6325	0.6187	0.6246
	DS-CNN	0.7246	0.7357	0.6983	0.7023	0.7135	0.6857	0.7129	0.7193	0.6874	0.7249
	DS-CNN_SE	0.7940	0.8167	0.7179	0.7881	0.7623	0.7087	0.8782	0.7627	0.8122	0.8266
OFC	Kmeans	0.5069	0.5793	0.5740	0.5820	0.5614	0.5419	0.5453	0.5901	0.5495	0.5074
	GMM	0.5831	0.5024	0.5841	0.5382	0.5576	0.5203	0.5192	0.5837	0.5327	0.5836
	GNBC	0.5197	0.5753	0.5623	0.5531	0.5843	0.5376	0.5631	0.5924	0.5624	0.5869
	LDA	0.5511	0.5817	0.5718	0.5313	0.5996	0.5710	0.5134	0.5936	0.5472	0.5738
	SVM	0.6496	0.6940	0.6079	0.6841	0.6623	0.6476	0.6881	0.6761	0.6357	0.6238
	Bayes	0.5126	0.5246	0.5313	0.5928	0.5532	0.5214	0.5492	0.5265	0.5253	0.5551
	DS-CNN	0.7365	0.7583	0.7639	0.7528	0.7429	0.7632	0.7639	0.7418	0.7649	0.7564
	DS-CNN_SE	0.8230	0.8190	0.8349	0.8429	0.8369	0.8530	0.8012	0.8865	0.8327	0.8448
FPC	Kmeans	0.5591	0.5492	0.5095	0.5413	0.5167	0.5258	0.5552	0.5996	0.5472	0.5313
	GMM	0.5769	0.5841	0.5764	0.5939	0.5642	0.5826	0.5696	0.5637	0.5758	0.5837
	GNBC	0.5632	0.5179	0.5835	0.5647	0.5361	0.5428	0.5642	0.5771	0.5493	0.5637
	LDA	0.5472	0.5413	0.5313	0.5258	0.5095	0.5096	0.5097	0.5492	0.5552	0.5591
	SVM	0.5623	0.5582	0.5702	0.5683	0.5484	0.5642	0.5623	0.5663	0.5642	0.5544
	Bayes	0.6754	0.6654	0.6595	0.6575	0.6536	0.6456	0.6198	0.6139	0.6080	0.6297
	DS-CNN	0.7643	0.7683	0.7439	0.7643	0.7629	0.7831	0.7594	0.7627	0.7583	0.7762
	DS-CNN_SE	0.8647	0.8627	0.8706	0.8577	0.8786	0.9107	0.8567	0.8488	0.8647	0.8873

Table 3. Statistics of classification accuracy of different algorithms.

Number	KMeans	GMM	GNBC	LDA	SVM	DS-CNN	DS-CNN_SE
1	0.5413	0.5618	0.5776	0.6429	0.6957	0.7724	0.8363
2	0.5540	0.5148	0.5325	0.6580	0.7057	0.8196	0.8669
3	0.5249	0.5754	0.5683	0.5942	0.6790	0.7874	0.8214
4	0.5377	0.5982	0.5242	0.6783	0.7383	0.7477	0.8851
5	0.5886	0.5298	0.5791	0.5752	0.7129	0.8214	0.8716
6	0.5978	0.5362	0.5927	0.5990	0.6735	0.7659	0.8847
7	0.5232	0.5816	0.5625	0.6396	0.6738	0.7847	0.8673
8	0.5539	0.5618	0.5817	0.5919	0.7239	0.8279	0.8757
9	0.5693	0.5283	0.5333	0.6624	0.6781	0.7546	0.8573
10	0.5797	0.6115	0.5792	0.5891	0.7347	0.7328	0.8659

### 3.2. Comparison of classification results of algorithms

The fNIRS sampling frequency was 8.13 Hz, channel selection was 26, and each participant had 56 trials of drug map stimulation data within 6 s, based on the sampling frequency  $\times$  the length of fNIRS data obtained in this way was 48 points. The ratio of the training set, validation set, and testing set was 7:2:1. After the final allocation, the training dataset consisted of 1680 trials, the validation dataset consisted of 448 trials, and the test dataset consisted of 224 trials. The network model, after later improvement, had a 1%–3% increase in classification accuracy compared to the original model. The use of neural network models was advantageous for evaluating the drug addiction level. Table 3 shows the accuracy statistics of different algorithms.

### 3.3. Discrimination evaluation

The confusion matrix of DS-CNN\_SE classification model is shown in Fig. 8. In the confusion matrix, 0 represents 0.5–5 years methamphetamine users, 1 represents 5–10 years methamphetamine users, and 2 represents 10–15 years methamphetamine users. In the classification of drug abuse, the classification

accuracy of 0.5–5 years was lower than that of 5–10 years and 10–15 years. 5–10 years and 10–15 years are basically correct in classification, and the prediction result of 10–15 years is slightly lower than that of 10–15 years, but it can still ensure high accuracy.

### 3.4. iCoh comparison between healthy people and drug user

Imaginary Part of Coherence (iCoh) is a measure of the linear relationship between two EEG channels at a specific frequency. iCoh is only sensitive to the synchronization of two electrode signals that lag each other.

Processing of data: (1) Extraction of EEG data, (2) Sampling frequency down to 250 Hz, (3) Band-pass filter: 0.5–45 Hz, (4) Trap band selection: 49–51 Hz, (5) Average reference, (6) ICA, (7) FCLAB toolbox processing, and (8) Taking Delta, Theta, Alpha, Beta, Gamma five bands of data for making statistical analysis.

Unpaired *t* test and *F* test to compare variances were utilized in the pair-wise comparison of methamphetamine users. *t*(df) = *t*-static, Unpaired *t* test, Two-tailed, *P* value < 0.0001 showed that the

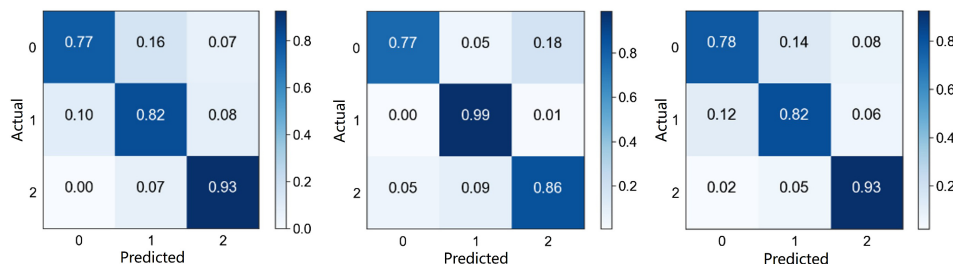


Fig. 8. Obfuscation matrix of classification model.

difference was statistically significant.  $F$  test to compare variances,  $F(DFn, Dfd) = F\text{-static}$ ,  $P$  value  $< 0.0001$  indicated the presence of significant difference.

In the comparison of drug addiction history of 0.5–5 years versus 5–10 years: For Delta, statistical analysis of combined Mean  $\pm$  SEM of column A,  $N = 2304$ ; and Mean  $\pm$  SEM of column B,  $N = 2304$  showed  $t(4606) = 26.57$ ,  $P < 0.001$ ;  $F(2303, 2303) = 1.933$ ,  $P < 0.0001$ . The same results were observed in Theta, Alpha, Beta, and Gamma. Finally, it can be found that in the comparison of drug addiction history of 0.5–5 years versus 5–10 years, there were significant differences in the five frequency bands of Delta, Theta, Alpha, Beta, and Gamma between any two participants. The iCoh of the brain network of healthy people and methamphetamine abusers varied across the five frequency bands under different drug addiction histories as follows.

In the Delta band, the highest for 10–15 years, followed by healthy people, followed by 0.5–5 years, and the lowest for 5–10 years. In the Theta band, the lowest at 5–10 years, followed by 0.5–5 years, followed by healthy people, and the highest at 10–15 years. In the Alpha band, the highest for 10–15 years, followed by 5–10 years, followed by healthy people, and the lowest for 0.5–5 years. In the Beta band, healthy people is the highest, followed by 5–10 years, followed by 10–15 years, and the lowest for 0.5–5 years. In the Gamma band, 0.5–5 years is the highest, followed by 10–15 years, followed by healthy people, and 5–10 years is the next lowest. Table 4 shows the five frequency bands of brain network change pattern of different drug addiction

history. Figure 9 shows the distribution of the five frequency bands of healthy people and abusers.

### 3.5. Changes of EEG topography map in healthy and drug users

According to the EEG topography map, the distribution of brain energy of healthy participants is even in the resting state, with their eyes closed. As the addiction history becomes longer, there are energy differences in the central area, parietal area, and temporal area of the brain. There is intense energy in the prefrontal cortex of the healthy projects in the resting state, with their eyes open. As the addiction history becomes longer, there are energy differences in the prefrontal cortex, central area, parietal area, occipital area and temporal area of the brain. Figures 10 and 11 show the EEG topography map in two resting states.

### 3.6. Statistical differences in fNIRS data with healthy people and methamphetamine users

The process of NIRS data processing is as follows: Use of DCT filter: Low-pass filter, high cutoff frequency (Hz): 0.1, high-pass filter, low cutoff frequency (Hz): 0.005. SNR threshold (dB): 30 Concentration baseline: spot. Spike removal: window: 10, STD threshold: 0.005.

Based on fNIRS data, the FPC functional area was selected, and the channel selection was 21, 22, 23, 24, 25, 26, 27, 28. Eight channels of HbO<sub>2</sub> data. 14 healthy people and 14 participants in each class at 0.5–5 years, 5–10 years, and 10–15 years.

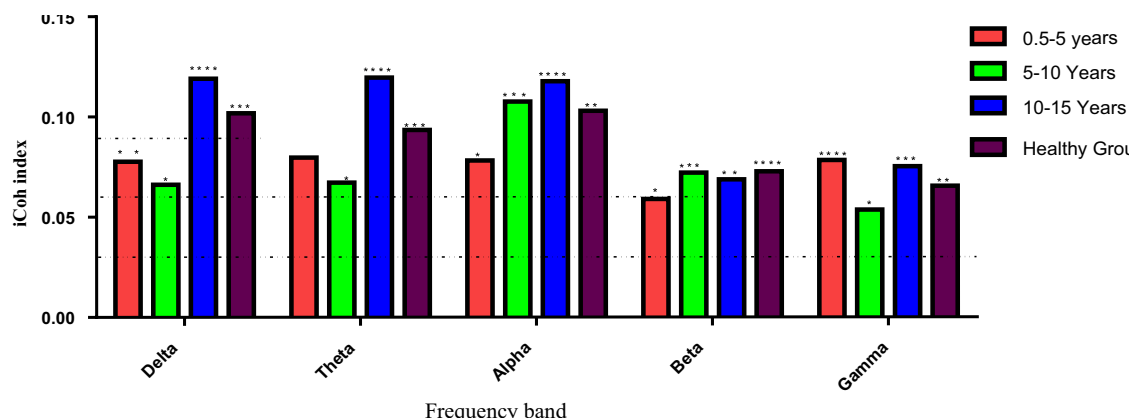


Fig. 9. The distribution of the five frequency bands of healthy people and abusers.

Table 4. Five frequency bands of brain network change pattern of different drug addiction histories.

Frequency band	Drug history	Minimum	25% Percentile	Median	75% Percentile	Maximum	Std. deviation	Std. error of mean	Mean
Delta	HCG	3.965e-010	0.06106	0.09827	0.1379	0.3364	0.05542	0.001066	0.1018***
	0.5-5	2.130e-010	0.04291	0.06944	0.1046	0.3109	0.04905	0.0009433	0.07765**
	5-10	3.940e-010	0.02771	0.05103	0.08664	0.2983	0.05454	0.001049	0.06617*
	10-15	3.744e-010	0.06925	0.1111	0.1643	0.3234	0.06631	0.001275	0.1190****
Theta	HCG	4.735e-011	0.04891	0.0818	0.1281	0.3600	0.05947	0.001144	0.09348***
	0.5-5	2.534e-010	0.03818	0.06721	0.1111	0.3166	0.05798	0.001115	0.07964**
	5-10	2.540e-011	0.01366	0.02498	0.04763	0.4632	0.1056	0.002030	0.06721*
	10-15	8.350e-011	0.07247	0.1144	0.1627	0.3660	0.06337	0.001219	0.1195****
Alpha	HCG	2.104e-010	0.06274	0.09730	0.1384	0.3359	0.05476	0.001053	0.1029**
	0.5-5	1.162e-010	0.04052	0.06832	0.1056	0.2627	0.05016	0.0009646	0.07823*
	5-10	6.420e-011	0.04678	0.07630	0.1183	0.5122	0.1016	0.001953	0.1075***
	10-15	2.595e-010	0.06583	0.1147	0.1622	0.3716	0.06426	0.001236	0.1177****
Beta	HCG	2.935e-011	0.04118	0.06975	0.09940	0.2609	0.04127	0.0007937	0.07263****
	0.5-5	1.105e-010	0.03218	0.05505	0.08068	0.2189	0.03540	0.0006808	0.05891*
	5-10	2.935e-010	0.04023	0.06509	0.09883	0.2741	0.04397	0.0008456	0.07207***
	10-15	1.253e-010	0.03900	0.06466	0.09730	0.1869	0.03868	0.0007439	0.06864**
Gamma	HCG	8.130e-011	0.03900	0.06194	0.08748	0.2310	0.03598	0.0006920	0.06548**
	0.5-5	1.761e-010	0.04125	0.06999	0.1116	0.2526	0.04868	0.0009361	0.07837****
	5-10	6.589e-011	0.02548	0.05045	0.07652	0.1803	0.03401	0.0006540	0.05360*
	10-15	1.123e-010	0.04356	0.06922	0.1008	0.2459	0.04336	0.0008339	0.07517***

The HbO<sub>2</sub> data of eight channels in the PFC functional area were taken out for each participant, and the data of 14 participants in each class were integrated together and the results in Table 5, the nonparametric test in One-Way ANOVA was used.

There were significant differences in brain PFC activation levels among healthy people and

methamphetamine users with different drug addiction history. The level of healthy people 0.004577 ± 0.0002673 mMol. At 0.5–5 years, the level of methamphetamine HbO<sub>2</sub>: 0.0004379 ± 0.009270 mMol/L; at 5–10 years, the level of HbO<sub>2</sub> in methamphetamine users was as follows: -0.0004974 ± 0.007861 mMol/L; at 10–15 years,

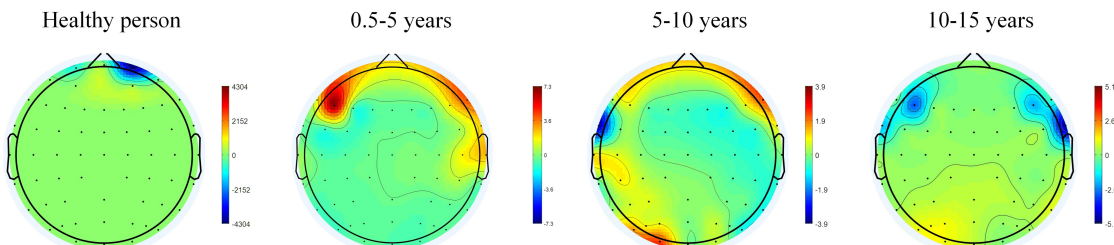


Fig. 10. EEG topography map of HCG and MUG in resting state with eyes closed.

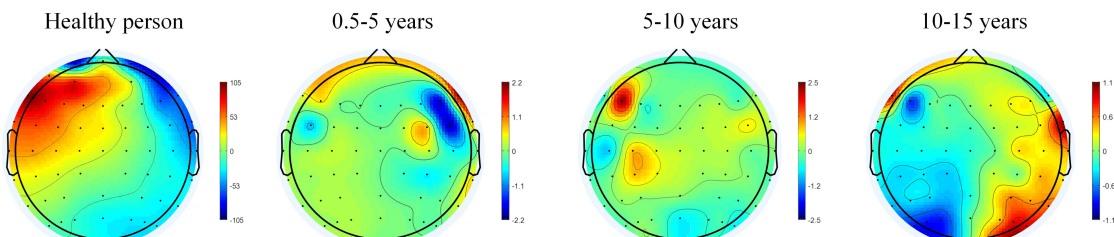


Fig. 11. EEG topography map of HCG and MUG in resting state with eyes open.

Table 5. Differences in FPC activation under different drug addiction histories.

Kruskal-Wallis test	
Exact or approximate <i>P</i> value?	Approximate
Do the medians vary signif. ( <i>P</i> < 0.05)	Yes
Number of groups	4
Kruskal-Wallis statistic	240.7
Number of values (total)	18816
<i>P</i> value	<i>P</i> < 0.0001

the level of HbO<sub>2</sub> in methamphetamine users was as follows:  $-0.001484 \pm 0.01297$  mMol/L. The law of HbO<sub>2</sub> activation for different addiction history was the highest for healthy people, followed by 0.5–5 years, followed by 5–10 years, and the lowest for 10–15 years.

According to the 3D activation map of the prefrontal cortex, the activation level in the prefrontal cortex of healthy participants is normal. As the addiction history becomes longer, the activation level becomes lower. Figure 12 shows 3D activation map of healthy people and addicts.

#### 4. Discussion

Methamphetamine is the most commonly abused drug worldwide. Long-term drug addiction can alter the brain function. EEG, fNIRS, and CNN were used in this study to analyze healthy controls and methamphetamine users.

We concluded that a long addiction history considerably affected the brain. This finding is consistent with that reported in previous studies on drug rehabilitation. Nevertheless, there were some differences between the results of this and previous studies: (1) Most researchers used only one type of device, whereas this research used EEG and fNIRS, improving the credibility of the results; (2) the iCoh in EEG was used to verify the differences in brain function across bands, which were caused by

different addiction histories. FPC activation on fNIRS was used to monitor methamphetamine users. An artificial intelligence-based algorithm was used for the first time to classify methamphetamine users with different addiction histories.

The long history of amphetamine use was associated with great activations of the prefrontal cortex.<sup>29</sup> According to London *et al.*, people with a long history of methamphetamine use often exhibit several signs of cortical and striatal dysfunctions.<sup>30</sup> In decision making, participants with previous drug use showed relatively more activation in the left OFC.<sup>31</sup> The dysfunction of interhemispheric connectivity of the insula and of the inferior frontal gyrus, to a lesser extent, is related to drug abuse in psychiatric populations.<sup>32</sup> Yamamoto *et al.* in their study of addiction history, observed that smoking exposure history influences serum nicotine levels and the brain's response to nicotine.<sup>33</sup> Methamphetamine use history has a significant influence on EEG and aggravates the changes in fNIRS activation.

Significant differences in brain functions were observed between healthy participants and methamphetamine users, verifying the harm of drug use and the challenges of rehabilitation.

The three-class accuracy pattern drawn with the Kmeans, GMM, LDA, SVM, Bayes, and CNN algorithms using the drug image showed that the accuracy in the OFC and FPC was significantly higher than that induced by the neutral image.

Drug clues have accurate induction on addiction characteristics. With prominent addiction characteristics, traditional classifiers, such as CNN, effectively chose reliable characteristics. The interpretability of machine learning was verified in this study.

Kmeans, GMM, GNBC, LDA, SVM, and Bayes, the traditional classic classification algorithms, offered no benefits in classifying different addiction histories. However, CNN, the most popular

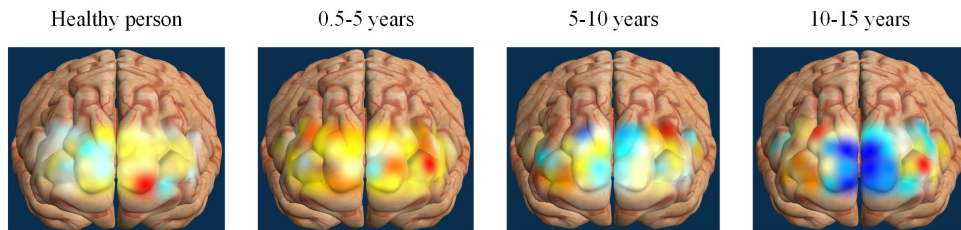


Fig. 12. 3D activation map of healthy people and addicts.

algorithm, was beneficial. For example, CNN directly entered the original data, extracted and optimized the features of a network, and effectively extracted the features by implicitly learning the feature patterns from the training data. CNN also performed well in solving problems related to the classification of high-dimensional features. Therefore, this method effectively extracted the effects of drug use on the brain by learning the underlying NIR data and classifying the physiological features. CNN improved the three-class accuracy of the different addiction histories. These findings demonstrate the objective effect of addiction time on the human body.

While in our study, the emphasis was the differences in the brain function problems in drug users with different histories of methamphetamine use. The control group was set and divided according to the length of drug use history of methamphetamine users (i.e., healthy people:  $n = 14$ ; addiction history: 0.5–5 years:  $n = 14$ ; 5–10 years:  $n = 14$ ; and 10–15 years:  $n = 14$ ). Through the comparison of the control group, it is found that after methamphetamine addiction, the impact on the brain changes with the increase of use time.

At present, in the study of addiction, various studies have compared drug addicts with healthy participants, drug addiction with nicotine, alcohol, etc. Some other researchers have analyzed the correlation between drug addiction and depression, drug addiction, and schizophrenia. However, currently, there are no targeted researches, only studies focusing on the use of methamphetamine drugs, and the history of methamphetamine addiction was 0.5–15 years. Within this range, methamphetamine users show the continuous habit of using drugs without stopping.

A limitation of this study is that only iCoh was used in the EEG analysis. Furthermore, the fNIRS data only included the FPC. Other physiological indicators must be analyzed to explore the effect of drug use on the brain.

The findings of this study will provide a theoretical reference for researchers and medical workers and will help in the development of customized rehabilitation therapies. This drug rehabilitation study aims to discover the mechanism of brain function after drug addiction, to develop novel techniques for drug addiction rehabilitation treatment, and to help drug users get rid of the addiction and embrace society and their families again.

## 5. Conclusions

This paper revealed how drug use history affects the brain functions of human beings by comparing healthy control groups (HCGs) and methamphetamine user groups (MUGs). The EEG and fNIRS data showed changes in the brain functional connections and brain activations caused by drug use history. The findings enrich the research regarding the relationship between neuronal activities and drug use history among methamphetamine users.

Unlike existing studies, this research combined EEG and fNIRS with traditional algorithm and machine learning. Long-term methamphetamine use results in brain function changes, which is consistent with previous findings. Conclusions on methamphetamine use are drawn by studying a large sample size with a long drug use history, providing theoretical references for the rehabilitation scheme design.

## Funding

This project was supported by Shanghai Municipal Science and Technology Plan Project (No. 22010502400), National Natural Science Foundation of China (Nos. 82072228, 92048205, and 62376149).

## Acknowledgments

The authors thank the Shanghai Drug Rehabilitation Administration Bureau and Shanghai Qing-dong Drug Rehabilitation Center for their support, and all the people who contributed to the writing of this paper.

## Conflicts of Interest

All contributing authors have no conflict of interests.

## ORCID

Xuelin Gu  <https://orcid.org/0000-0002-0014-7278>  
Xiaou Li  <https://orcid.org/0000-0002-3172-7507>  
Banghua Yang  <https://orcid.org/0000-0002-8561-5631>

## References

1. S. Yasin, S. A. Hussain, S. Aslan, I. Raza, M. Muzammel, A. Othmani, “EEG based major

- depressive disorder and bipolar disorder detection using neural networks: A review," *Comput. Meth. Prog. Biomed.* **202**, 106007 (2021).
2. B. Boloukian, F. Safi-Esfahani, "Recognition of words from brain-generated signals of speech-impaired people: Application of autoencoders as a neural Turing machine controller in deep neural networks," *Neural Netw.* **121**, 186–207 (2020).
  3. F. Molinari, U. R. Acharya, R. J. Martis, R. De Luca, G. Petraroli, W. Liboni, "Entropy analysis of muscular near-infrared spectroscopy (NIRS) signals during exercise programme of type 2 diabetic patients: Quantitative assessment of muscle metabolic pattern," *Comput. Methods. Programs Biomed.* **112**(3), 518–528 (2013).
  4. M. Ferrari, V. Quaresima, "A brief review on the history of human functional near infrared spectroscopy (fNIRS) development and fields of application," *Neuroimage* **63**(2), 921–935 (2012).
  5. R. Pascual-Marqui, "Assessing direct paths of intracortical causal information flow of oscillatory activity with the isolated effective coherence (iCoh)," *Front Hum Neurosci.* **8**(448), 1–12 (2014).
  6. P. Mirzaei *et al.*, "Surrogate data test for nonlinearity of EEG signals: A newborn EEG burst suppression case study," *Digital Signal Process.* **70**, 30–38 (2017).
  7. R. D. Pascual-Marqui *et al.*, "Assessing direct paths of intracortical causal information flow of oscillatory activity with the isolated effective coherence (iCoh)," *Front. Human Neurosci.* **8**, 448 (2014).
  8. L. Zhang *et al.*, "Enhanced high-frequency precuneus-cortical effective connectivity is associated with decreased sensory gating following total sleep deprivation," *NeuroImage* **197**, 255–263 (2019).
  9. S. Steinmann *et al.*, "The callosal relay model of interhemispheric communication: New evidence from effective connectivity analysis," *Brain Topograp.* **31**(4), 218–226 (2018).
  10. B. B. Jorge *et al.*, "Resting EEG effective connectivity at the sources in developmental dysphonetic dyslexia. Differences with non-specific reading delay," *Int. J. Psychophysiol.* **153**, 135–147 (2020).
  11. J. M. Schoffelen, J. Gros, "Source connectivity analysis with MEG and EEG," *Hum. Brain Mapp.* **30**(6), 1857–1865 (2009).
  12. A. C. Ehli, S. Schneider, T. Dresler, A. J. Fallgatter, "Application of functional near-infrared spectroscopy in psychiatry," *NeuroImage*, **85**, 478–488 (2014).
  13. A. S. Huhn, M. M. Sweeney, R. K. Brooner, M. S. Kidorf, D. A. Tompkins, H. Ayaz, K. E. Dunn, "Prefrontal cortex response to drug cues, craving, and current depressive symptoms are associated with treatment outcomes in methadone-maintained patients," *Neuropsychopharmacology* **44**(4), 826–833 (2019).
  14. J. L. Stewart, A. C. May, R. L. Aupperle, J. Bodurka, "Forging neuroimaging targets for recovery in opioid use disorder," *Front. Psychiatry* **10**, 117 (2019).
  15. L. H. Ernst, M. M. Plichta, E. Lutz, A. K. Zesewitz, S. V. Tupak, T. Dresler, A.-C. Ehli, A. J. Fallgatter, "Prefrontal activation patterns of automatic and regulated approach-avoidance reactions — A functional near-infrared spectroscopy (fNIRS) study," *Cortex* **49**(1), 131–142 (2013).
  16. N. Okada *et al.*, "Characterizing prefrontal cortical activity during inhibition task in methamphetamine-associated psychosis versus schizophrenia: A multi-channel near-infrared spectroscopy study," *Addict. Biol.* **21**(2), 489–503 (2016).
  17. W. Asim *et al.*, "Multiday evaluation of techniques for EMG based classification of hand motions," *IEEE J. Biomed. Health Inf.* **23**(4), 1526–1534 (2018).
  18. Z. Huang *et al.*, "Similarity measure between patient traces for clinical pathway analysis: Problem, method, and applications," *IEEE J. Biomed. Health Inf.* **18**(1), 4–14 (2014).
  19. J. Meng *et al.*, "Improved semisupervised adaptation for a small training dataset in the brain–computer interface," *IEEE J. Biomed. Health Inf.* **18**(4), 1461–1472 (2014).
  20. Y. Lei, T. Yang, A. B. Chan, "Density-preserving hierarchical EM algorithm: Simplifying Gaussian mixture models for approximate inference," *IEEE Trans. Pattern Anal. Mach. Intell.* **41**(6), 1323–1337 (2018).
  21. N. Vlassis, A. Likas, "A kurtosis-based dynamic approach to Gaussian mixture modeling," *IEEE Trans. Syst. Man Cybern. A, Syst. Humans* **29**(4), 393–399 (1999).
  22. J. J. Whang *et al.*, "Non-exhaustive, overlapping clustering," *IEEE Trans. Pattern Anal. Mach. Intell.* **41**(11), 2644–2659 (2019).
  23. R. Zhang *et al.*, "Joint learning of fuzzy K-Means and nonnegative spectral clustering with side information," *IEEE Trans. Image Process.* **28**(5), 2152–2162 (2019).
  24. S. Maldonado, J. M. Merigo, J. Miranda, "IOWA-SVM: A density-based weighting strategy for SVM classification via OWA operators," *IEEE Trans. Fuzzy Syst.* **28**(9), 2143–2150 (2019).
  25. S. Chen, C. Gao, "Linear priors mined and integrated for transparency of blast furnace black-box SVM model," *IEEE Trans. Ind. Inf.* **16**(6), 3862–3870 (2020).
  26. M. Capdevila, O. W. Márquez Flórez, "A communication perspective on automatic text categorization,"

- IEEE Trans. Knowl. Data Eng.* **21**(7), 1027–1041 (2009).
27. S. C. Markley, D. J. Miller, “Joint parsimonious modeling and model order selection for multivariate Gaussian mixtures,” *IEEE J. Sel. Top. Signal Process.* **4**(3), 548–559 (2010).
28. G. Nolte *et al.*, “Identifying true brain interaction from EEG data using the imaginary part of coherency,” *Clin. Neurophysiol.* **115**(10), 2292–2307 (2004).
29. J. Guterstam *et al.*, “Cue reactivity and opioid blockade in amphetamine dependence: A randomized, controlled fMRI study,” *Drug Alcohol Depend.* **191**, 91–97 (2018).
30. E. D. London, M. Kohno, A. M. Morales, M. E. Ballard, “Chronic methamphetamine abuse and corticostriatal deficits revealed by neuroimaging,” *Brain Res.* **1628**, 174–185 (2015).
31. K. D. Ersche, P. C. Fletcher, S. J. G. Lewis, L. Clark, G. Stocks-Gee, M. London, “Abnormal frontal activations related to decision-making in current and former amphetamine and opiate dependent individuals,” *Psychopharmacol.* **180**(4), 612–623 (2005).
32. H. Viswanath, K. M. Velasquez, R. Savjani, D. L. Molfese, K. Curtis, P. J. Molfese, “Interhemispheric insular and inferior frontal connectivity are associated with substance abuse in a psychiatric population,” *Neuropharmacology* **92**, 63–68 (2015).
33. R. T. Yamamoto, M. L. Rohan, N. Goletiani, D. Olson, M. Peltier, P. F. Renshaw, “Nicotine related brain activity: The influence of smoking history and blood nicotine levels, an exploratory study,” *Drug Alcohol Depend.* **129**(1), 137–144 (2013).